Available online at website: https://journal.bcrec.id/index.php/bcrec

Bulletin of Chemical Reaction Engineering & Catalysis, 20 (4) 2025, 750-756

Original Research Article

Tailoring Bandgap and Crystallinity of TiO_2 via Mg Doping for Enhanced DSSC Photoanode Performance

Mursal Mursal*, Malahayati Malahayati, Ismail Ismail, Irhamni Irhamni, Zulkarnain Jalil

Department of Physics, Faculty of Mathematics and Natural Sciences, Universitas Syiah Kuala, Banda Aceh 23111, Indonesia.

Received: 12th April 2025; Revised: 16th October 2025; Accepted: 17th October 2025
Available online: 21th October 2025; Published regularly: December 2025

Abstract

The structural and optical properties of magnesium-doped titanium dioxide (Mg–TiO_2) nanocrystalline films were investigated for potential application as photoanodes in dye-sensitized solar cells (DSSCs). The films were synthesized via a sol-gel method using titanium(IV) isopropoxide and magnesium acetate as precursors. Mg doping concentrations ranging from 0 to 4 mol% were explored. The films were deposited onto glass substrates using the doctor blade technique and annealed at various temperatures. Characterization was carried out using X-ray diffraction (XRD), scanning electron microscopy with energy-dispersive X-ray spectroscopy (SEM-EDS), Fourier-transform infrared spectroscopy (FTIR), and UV–Vis spectroscopy. XRD analysis confirmed the formation of TiO_2, MgO, and $MgTiO_3$ phases, with a notable decrease in crystallite size as Mg content increased. The smallest crystallite size of 12.71 nm was obtained at 4 mol% Mg doping. SEM images revealed improved surface morphology and more uniform porosity in doped films. FTIR spectra indicated no significant changes in chemical bonding, while UV–Vis analysis showed a decrease in bandgap energy from 3.8 eV to 3.4 eV with Mg doping. These modifications suggest enhanced dye adsorption and reduced charge recombination, indicating the potential of Mg-doped TiO_2 films to improve DSSC performance.

Keywords: Mg-doped TiO_2; sol–gel method; crystallite size; photoanode; dye-sensitized solar cell

How to Cite: Mursal, M., Malahayati, M., Ismail, I., Irhamni, I., Jalil, Z. (2025). Tailoring Bandgap and Crystallinity of TiO_2 via Mg Doping for Enhanced DSSC Photoanode Performance. *Bulletin of Chemical Reaction Engineering & Catalysis*, 20 (4), 750-756. (doi: 10.9767/bcrec.20473)

Permalink/DOI: https://doi.org/10.9767/bcrec.20473

1. Introduction

Dye-sensitized solar cells (DSSCs) remain a promising and evolving technology due to several advantages over conventional silicon-based solar cells [1]. These advantages include low production cost, simple fabrication, environmental friendliness, and relatively high conversion efficiency [2,3]. A typical DSSC is composed of four main components: a transparent conductive substrate coated with a semiconductor layer serving as the photoanode, a dye-sensitizer that absorbs light, an electrolyte that facilitates charge transport, and a counter electrode with an electrocatalyst that completes the circuit by transferring electrons back from the external load [3]. The conversion of sunlight (photons) into electrical energy in a DSSC primarily depends on the efficiency of the dye and the surface area and porosity of the semiconductor nanomaterial used in the photoanode [2]. However, performance is limited by charge recombination at the semiconductor/dye/electrolyte interface.

Titanium dioxide (TiO_2) is one of the most widely used photoanode materials in DSSCs due to its suitable bandgap, chemical stability, non-toxicity, and availability [1,4–6]. Despite these advantages, TiO_2 suffers low photon absorption and low electric conductivities [7], and suffers from fast charge recombination, which limits the overall efficiency of the DSSC [8]. The structural

* Corresponding Author.
Email: mursal@usk.ac.id (M. Mursal)

and morphological properties of TiO_2, such as its crystal structure, grain size, and surface roughness, directly influence dye adsorption, electron injection, charge transport, and recombination dynamics.

One strategy to enhance TiO_2 performance is metal doping, which introduces new energy levels that can act as traps or acceptors for photogenerated electrons, thus reducing recombination [9,10]. Doping can also narrow the bandgap and enhance photon absorption. Metals such as Pt, Ni, Cu, Zn, Zr, La, Ce, and Fe have been explored as dopants [9,11–13]. Recent studies have also shown that magnesium (Mg) is a promising dopant for improving the optical and electronic properties of TiO_2. Mg cation (0.72 Å) has an atomic radius slightly larger than the Ti cation (0.64 Å) which makes the Mg a good candidate for doping to adjust bandgap alignment [7,14].

TiO_2 thin films can be synthesized using various techniques, including the sol-gel method [2,12,15–20]. This technique enables low-temperature processing and good compositional control. However, sol–gel-derived TiO_2 often has low crystallinity due to the rapid hydrolysis of precursors and insufficient condensation during drying. Optimization of synthesis and deposition parameters is therefore necessary to enhance film quality.

In this study, Mg-doped TiO_2 films were synthesized via a sol-gel method, using titanium(IV) isopropoxide and magnesium acetate as precursors. The Mg doping concentration was varied from 0 to 4 mol%. The films were deposited on glass substrates using the doctor blade technique and characterized using XRD, SEM-EDS, and UV–Vis spectroscopy to evaluate their structural, morphological, and optical properties.

2. Materials and Methods

2.1 Materials

Titanium(IV) isopropoxide (TTIP), magnesium acetate tetrahydrate, isopropanol, hydrochloric acid (HCl), ethanol, acetic acid, and Triton X-100 were obtained from commercial suppliers and used without further purification. All chemicals were of analytical grade, and deionized water was used in all preparation steps.

2.2 Synthesis of Mg-Doped TiO_2 Powder

Mg-doped TiO_2 powders were synthesized via a modified sol-gel method. First, 10 mL of titanium(IV) isopropoxide was slowly added to 30 mL of isopropanol under continuous magnetic stirring. Separately, magnesium acetate tetrahydrate was dissolved in a mixture of deionized water and hydrochloric acid, with the Mg concentration adjusted to 0, 2, and 4 mol% relative to Ti.

The magnesium precursor solution was added dropwise into the TTIP solution, and the mixture was stirred for 2 hours at room temperature until a gel formed. The gel was aged for 24 hours, then dried at 60 °C for 12 hours. The resulting xerogel was washed with ethanol, dried again, and finally calcined at 500 °C for 5 hours in a muffle furnace to obtain the crystalline Mg-doped TiO_2 powders.

2.3 Fabrication of Thin Films

The synthesized powders were mixed with ethanol, acetic acid, and a small amount of Triton X-100 to form a homogenous slurry. The slurry was applied onto clean glass substrates using the doctor blade technique. The films were then air-dried and annealed at 450 °C for 2 hours to enhance crystallinity and adhesion to the substrate.

2.4 Characterization Techniques

Structural analysis was conducted using a Shimadzu XRD-7000 diffractometer with CuKα radiation (λ = 1.5406 Å). The given voltage was 40 kV, the current was 30 mA, and the detected angle (2θ) was set from 10 to 80^0. The average crystallite size was calculated using the Scherrer equation [21]. Scanning Electron Microscopy (SEM) and Energy-Dispersive X-ray Spectroscopy (EDS) were used to analyze the surface morphology and elemental composition of Mg-doped TiO2. Moreover, Fourier-Transform Infrared Spectroscopy (FTIR) was used to record the spectra in the range of 400–4000 cm^{-1} to identify functional groups and bonding characteristics. The optical absorption spectra were obtained using a Shimadzu UV-1800 spectrophotometer. The optical bandgap was calculated using Tauc plots based on the absorbance data. The absorption coefficient (α) was calculated using the relation: $\alpha = -1/d \ln T(\lambda)$, where d is the thickness and T is the optical transmittance of the films. The optical bandgap was determined using the expression $\alpha h\nu = A\ (h\nu - E_g)^m$, where A is a constant and m is equal to ½ for the indirect gap and 2 for the direct gap. The bandgap energy was determined using plot of $(\alpha h\nu)1/m$ vs. photon energy ($h\nu$) [11].

3. Results and Discussion

The structure and crystal size of the Mg-doped TiO_2 films were characterized using XRD (Shimadzu with CuKα radiation λ = 1.54060 Å). The applied voltage is 40 kV, the current is 30 mA, and the detected angle (2θ) is 10^o to 80^0. Identification of the phases formed in the sample through XRD pattern analysis and XRD data with respect to the detected 2θ angle, lattice distance

factor (*d*), intensity (I / II), and crystal phase. The database from PDF (powder diffraction file) - ICDD (International Center for Diffraction Data) was used for matching XRD results. Based on the matching that has been done, it shows that the phase peaks of the XRD results are in accordance with the PDF-ICDD data base. The 2θ value of each sample measured corresponds to the 2θ angle value stated in the ICDD standard, as shown in Figure 1.

We found that there are three phases of compounds, namely TiO_2, MgO, and $MgTiO_3$. The most diffraction peak that appears is TiO_2, this is influenced by the large concentration of TiO_2 in the sample. The highest TiO_2 peak was observed at an angle of 25.2580 in pure TiO_2, also in Mg doped TiO_2 samples. TiO_2 peak was observed at 25.3380, 25.2902, 25.3238, and 25.3137. The MgO peak appears at an angle of 62.1883 of each sample that is doped by Mg. It appears that the height of the main peak in the x-ray diffraction pattern of the sample is very different as shown in Figure 2. This difference in the height of the diffraction peaks indicates a difference in the degree of crystallization of the samples [12]. Samples that are annealed at 600 ^{0}C have a better degree of crystallization.

The crystal size of a material is strongly influenced by the FWHM values. Each of samples has a different diffraction peak width so that the FWHM values are also different. The wider the diffraction peak of the material, the greater the value of FWHM so it also determines the size and size of the crystal. The crystal size of the samples are shown in Table 1.

We found that the largest crystal size of 18.98 nm produced from pure TiO_2 sample, with a FWHM value of 0.45120. While the smallest crystal size of 12.71 nm was obtained from sample with 4% mol Mg doped correspond to the smallest FWHM value of 0.67500. Reducing in the size of the crystals in the sample probably reduce the recombination and expand the surface of the sample so that the ability to absorb sunlight energy was improved.

Surface morphology of the Mg-doped TiO_2 films were analyzed using an electron microscope (SEM) Hitachi Tabletop Microscope TM 3000. The surface morphology of pure TiO_2 and Mg doped TiO_2 samples were shown in Figure 3. We observed that the surface of TiO_2 and Mg doped TiO_2 were still rather rough, and the pore size is not homogeneous. This is indicated that the process of films forming is still imperfect.

Table 1. The Crystals size of TiO_2 and Mg doped TiO_2 films.

Sample	Parameters		
	FWHM (°)	θ (°)	Crystal size (nm)
Pure TiO_2	0.45120	12.629	18.98
TiO_2:Mg 1% mol	0.46630	12.669	18.52
TiO_2:Mg 2% mol	0.63080	12.6451	13.64
TiO_2:Mg 3% mol	0.59140	12.6619	14.56
TiO_2:Mg 4% mol	0.67500	12.65685	12.71

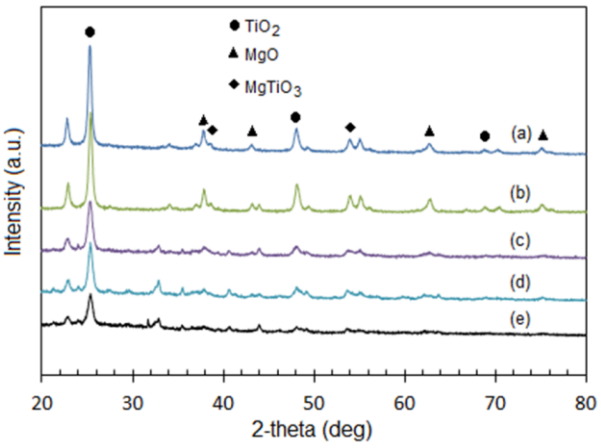

Figure 1. X-ray diffraction pattern from samples (a) pure TiO_2, (b) 1% mol Mg doped TiO_2, (c) 2% mol Mg doped TiO_2, (d) 3% mol Mg doped TiO_2, (e) 4% mol of Mg doped TiO_2.

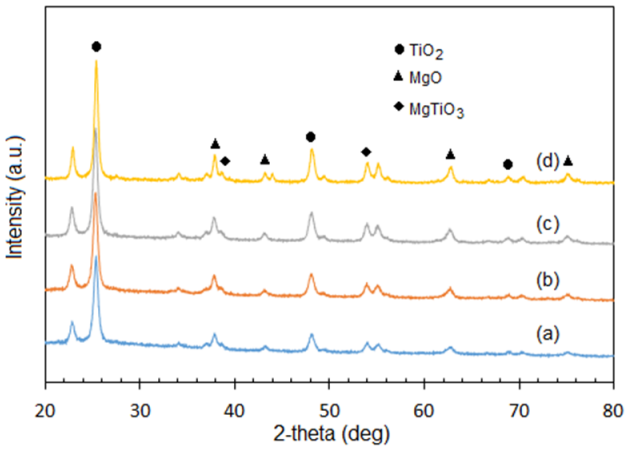

Figure 2. X-ray diffraction pattern of 4% Mg-doped TiO_2 annealed at varying temperatures, (a) 400 ^{0}C, (c) 450 ^{0}C, (d) 500 ^{0}C, (e) 600 ^{0}C.

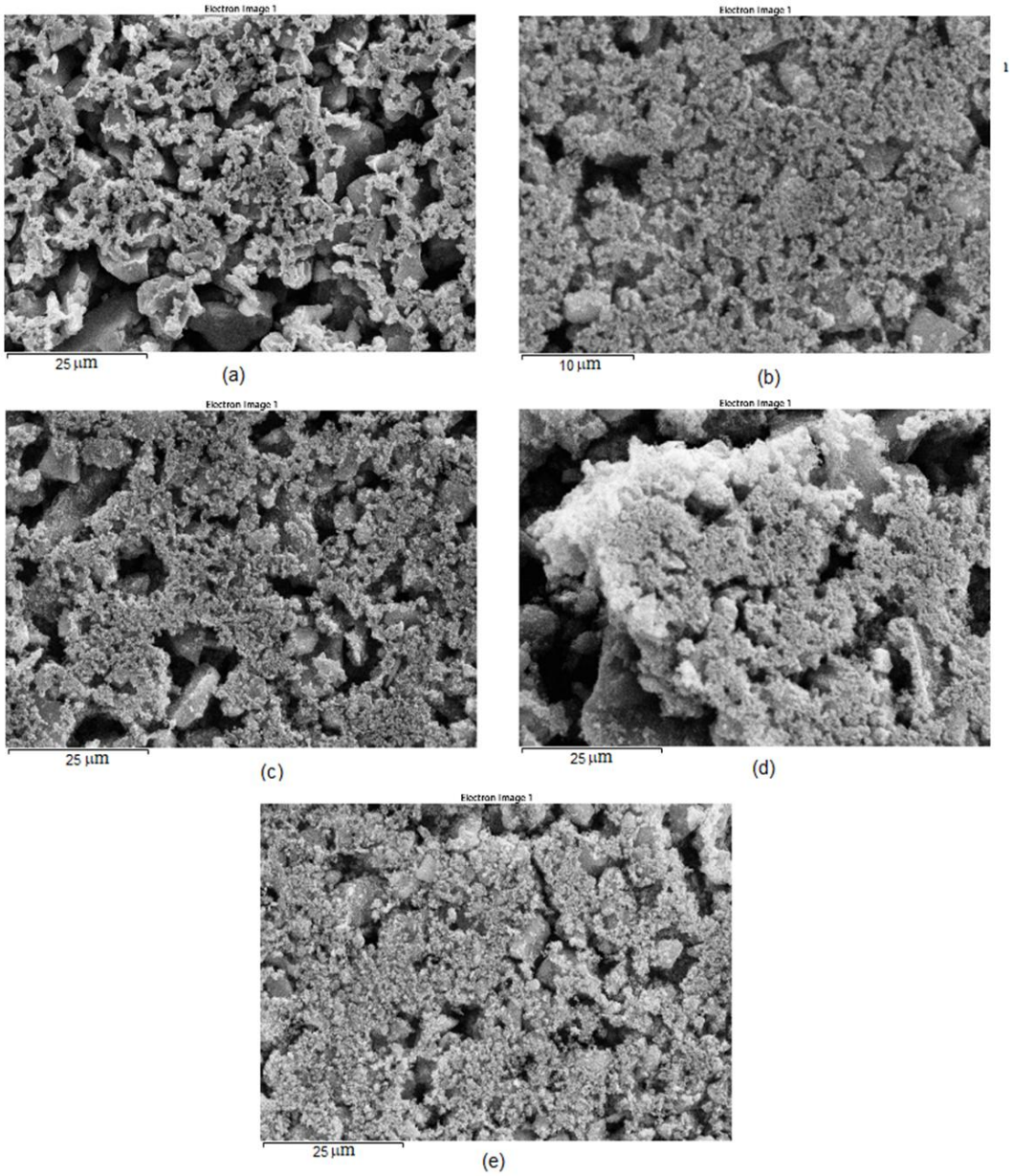

Figure 3. SEM photographs of samples (a) pure TiO_2, (b) 1% mol Mg doped TiO_2, (c) 2% mol Mg doped TiO_2, (d) 3% mol Mg doped TiO_2, and (e) 4% mol Mg doped TiO_2 at 5000x magnification.

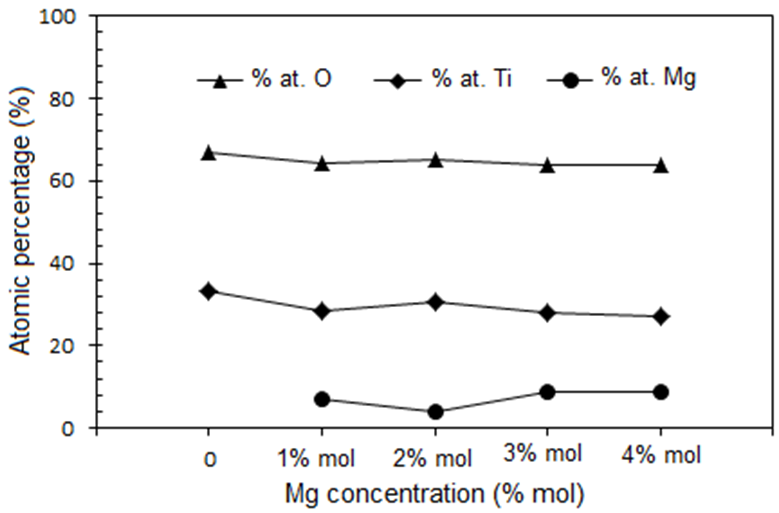

Figure 4. Effect of Mg concentration on the atomic percentage of the elements contained in the sample.

However, a TiO_2 film doped with 4% mol Mg showed a more uniform surface and more uniform pore size than the others. We can conclude that the addition of Mg can improve the surface morphology and porosity of the Mg doped TiO_2 film.

The doping of Mg into TiO_2 influences the atomic percentage of the elements contained in the sample. The doping of Mg not only increases the percentage of Mg atoms, but also alters the percentage of Ti and O atoms in the samples. The percentage of Ti atoms decreases with increasing percentage of Mg atoms. However, the percentage of O atoms does not change significantly with increasing percentage of Mg atoms. This deterioration showed that Mg atom could replace the Ti atoms.

FTIR spectra of pure TiO_2 and Mg doped TiO_2 are shown in Figure 5. The presence of Ti-O-Ti and Ti-O polymer chains can be observed at the wave numbers of 471 and 789 cm^{-1}. Ti-O-O band vibrations were identified at wave number 693 cm^{-1}. Ti-O-C stretching appears at wave numbers 1009, 1122 and 1138 cm^{-1}. While the widening of the band from wave numbers 3000 to 3600 cm^{-1} is related to the vibration stretching mode of the hydroxyl group. It was seen that there were no significant differences in the FTIR patterns of the two samples. However, the value of the percentage of transmittance of the Mg doped TiO_2 sample is higher than that of pure TiO_2.

UV-Vis spectra of pure TiO_2 and 4% mol Mg doped TiO_2 as a function of photon wavelength is shown in Figure 6. We found that the optical bandgap of these films are 3.8 eV and 3.4 eV, respectively. From this result, it was clear that doping Mg into TiO_2 had narrowed the energy gap of the Mg/TiO_2 film and reveal premature recombination in the cell, so that the resulting higher efficiency DSSC.

4. Conclusion

Mg-doped TiO_2 films were successfully synthesized using a modified sol–gel method and deposited via the doctor blade technique. Structural analysis confirmed the formation of TiO_2, MgO, and $MgTiO_3$ phases, with a reduction in crystallite size as Mg concentration increased. The smallest crystallite size of 12.71 nm was obtained at 4 mol% Mg doping, which is beneficial for enhancing surface area and dye adsorption. SEM analysis revealed improved surface morphology and more uniform porosity with increasing Mg content. EDS confirmed the successful incorporation of Mg into the TiO_2 lattice, while FTIR showed no significant changes in chemical bonding. UV–Vis analysis demonstrated a reduction in the optical bandgap from 3.8 to 3.4 eV, indicating enhanced light-harvesting properties. These results suggest that Mg doping effectively tailors the structural and optical characteristics of TiO_2, improving its potential as a photoanode material for DSSC applications. Further studies involving electrochemical impedance spectroscopy (EIS) and photovoltaic performance testing are recommended to evaluate the charge transport dynamics and overall device efficiency.

Acknowledgment

ZJ special thanks to Séjour Scientifique de Haut Niveau (SSHN) Program 2024. Authors acknowledge Syarifah Fathmiyah (Materials Physics and Energy Laboratory, USK) for her assistances in XRD and SEM investigations.

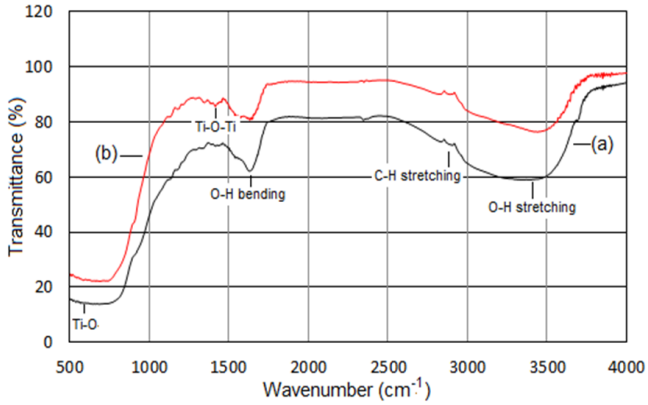

Figure 5. FTIR spectrum of (a) pure TiO_2 and (b) 4% mol Mg TiO_2 films.

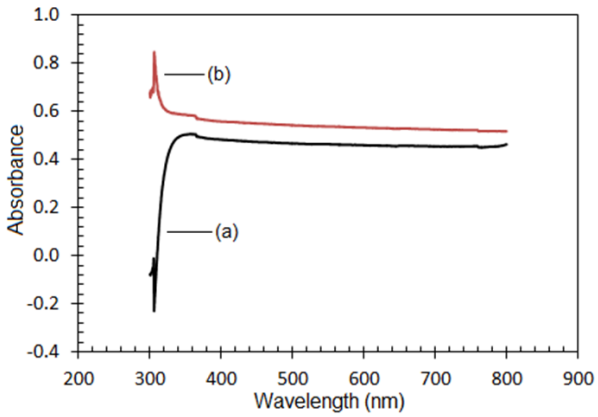

Figure 6. Absorbance of (a) pure TiO_2 and (b) 4% mol Mg doped TiO_2 as a function of photon wavelength.

CRedit Author Statement

Author Contributions: M. Mursal: Conceptualization, Methodology, Investigation, Data Analysis, Writing, Review and Editing; M. Malahayati: Methodology, Investigation, Data Curation, Writting Draft Preparation; I. Ismail: Validation, Data Curation; I. Irhamni: Investigation, Resources, Writing, Review and Editing; Z. Jalil: Review, Languange Modification, Validation. All authors have read and agreed to the published version of the manuscript. The authors have read and agreed to the published version of the manuscript.

References

[1] Chappidi, V.R., Seshaiah, K.V., Madduri, S., Raavi, S.S.K. (2024) Rare-earth-doped TiO2 photoanode DSSCs for indoor photovoltaics: a comparative study. *Journal of Materials Science: Materials in Electronics*, 35 (2024). DOI: 10.1007/s10854-024-12261-9.

[2] Aydın Ünal, F. (2025) Synthesis and characterization of the doped/co-doped SnO 2 nanoparticles by the sol–gel method. *Int. J. Appl. Ceram. Technol.*, 22 (2025). DOI: 10.1111/ijac.14916.

[3] Srivastava, K.V., Srivastava, P., Srivastava, A., Maurya, R.K., Singh, Y.P., Srivastava, A. (2025) 1D TiO2 photoanodes: a game-changer for high-efficiency dye-sensitized solar cells. *RSC Advances*, 15 (2025) 4789–4819. DOI: 10.1039/d4ra06254j.

[4] Al Moyeen, A., Mahmud, R.M., Mazumder, D.D., Ghosh, S., Datta, O., Molla, A., Begum, M.E. (2024) Investigation of structural, optical, antibacterial, and dielectric properties of sol-gel and biosynthesized TiO2 nanoparticles, *Heliyon*, 10. DOI: 10.1016/j.heliyon.2024.e40776.

[5] Matsunaga, M., Yu, Y., Takahashi, K. (2024). Photoelectrochemical Activity of TiO2/MWCNT Thin-Film Electrodes with Different Film Structures Prepared by Combining Electrophoretic Deposition and Sol–Gel Method. *Electrochemistry*, 92. DOI: 10.5796/electrochemistry.24-00014.

[6] Atia, D.M., Ahmed, N.M., Abou Hammad, A.A., Toraya, M.M., El Nahrawy, A.M. (2024) Enhanced performance of Mg and la co-doped TiO2(98%)-ZrO2(2%)photoanode for dye-sensitized solar cells. *Clean Energy*, 8 (2024) 225–236. DOI: 10.1093/ce/zkae091.

[7] Arshad, Z., Khoja, A.H., Shakir, S., Afzal, A., Mujtaba, M.A., Soudagar, M.E.M., Fayaz, H., Saleel C, A., Farukh, S., Saeed, M. (2021) Magnesium doped TiO2as an efficient electron transport layer in perovskite solar cells. *Case Studies in Thermal Engineering*, 26. DOI: 10.1016/j.csite.2021.101101.

[8] Dey, A., Vashishtha, L., Gogate, P.R. (2025). Ultrasound-assisted sol–gel synthesis of N-TiO2, Fe-TiO2, and TiO2 with application in treatment of a commercial effluent. *Journal of Chemical Technology and Biotechnology*, 100, 697-716. DOI: 10.1002/jctb.7808.

[9] Morante, N., Monzillo, K., Vaiano, V., Kadirova, Z.C., Sannino, D. (2025) Synthesis and Characterization of a Novel Sol–Gel-Derived Ni-Doped TiO2 Photocatalyst for Rapid Visible Light-Driven Mineralization of Paracetamol. *Nanomaterials*, 15. DOI: 10.3390/nano15070530.

[10] Lau, A., Goh, C.Y., Guo, Y., Alsultan, A.G., Taufiq-Yap, Y.H., Nurhadi, M., Lai, S.Y. (2025) Visible-light Degradation of Methylene Blue using Energy-Efficient Carbon-Doped TiO2: Kinetic Study and Mechanism. *Bulletin of Chemical Reaction Engineering & Catalysis*, 20 177–192. DOI: 10.9767/bcrec.20347.

[11] Stoyanova, A., Hitkova, H., Kaneva, N., Bachvarova-Nedelcheva, A., Iordanova, R., Marinovska, P. (2024) Photocatalytic Degradation of Paracetamol and Antibacterial Activity of La-Modified TiO2 Obtained by Non-Hydrolytic Sol–Gel Route. *Catalysts*, 14. DOI: 10.3390/catal14080469.

[12] Yang, F., Wang, C., Li, L., Diao, H., Wang, Y., Zheng, X., Li, C. (2025) Nickel-Doped TiO2 Nanoplate Synthesized via Mechanical Ball Milling-Assisted Sol–Gel Method for Photocatalytic Degradation of MB and NO. *Processes*, 13. DOI: 10.3390/pr13041192.

[13] Khalaghi, M., Atapour, M., Momeni, M.M., Karampoor, M.R. (2025) Visible light photocatalytic efficiency and corrosion resistance of Zn, Ni, and Cu-doped TiO2 coatings. *Results Chem.*, 13. DOI: 10.1016/j.rechem.2025.102032.

[14] Bharatbhai Akhani, S., Kumar Thatikonda, S., Solanki, M.B., Akhani, T., Gone, S., Singh Rathore, M. (2024) Photoluminescence and photocatalytic activity of sol gel synthesized Mg doped TiO2 nanoparticles. *Inorg. Chem. Commun.*, 170. DOI: 10.1016/j.inoche.2024.113294.

[15] Flores-Gómez, J., Mota-Macías, S., Guerrero-Jiménez, J.P., Romero-Arellano, V.H., Morales-Rivera, J. (2024) Sol–Gel Synthesis of TiO2 with Pectin and Their Efficiency in Solar Cells Sensitized by Quantum Dots. *Gels*, 10. DOI: 10.3390/gels10070470.

[16] Vlăduţ, C.M., Anastasescu, C., Preda, S., Mocioiu, O.C., Petrescu, S., Pandele-Cusu, J., Culita, D., Bratan, V., Balint, I., Zaharescu, M. (2024) Mn-doped ZnO nanopowders prepared by sol–gel and microwave-assisted sol–gel methods and their photocatalytic properties. *Beilstein Journal of Nanotechnology*, 15, 1283–1296. DOI: 10.3762/bjnano.15.104.

[17] Ivanova, T., Harizanova, A., Koutzarova, T., Closset, R. (2024) Crystallization and Optical Behaviour of Nanocomposite Sol-Gel TiO2:Ag Films. *Molecules*, 29. DOI: 10.3390/molecules29215156.

[18] Ćurković, L., Briševac, D., Ljubas, D., Mandić, V., Gabelica, I. (2024) Synthesis, Characterization, and Photocatalytic Properties of Sol-Gel Ce-TiO2 Films, *Pre Pprints*. DOI: 10.20944/preprints202405.0652.v1.

[19] Sadek, O., Touhtouh, S., Rkhis, M., Anoua, R., El Jouad, M., Belhora, F., Hajjaji, A. (2022) Synthesis by sol-gel method and characterization of nano-TiO2 powders. *Materials Today Proceeding*, 456–458. DOI: 10.1016/j.matpr.2022.06.385.

[20] Podelinska, A., Neilande, E., Pankratova, V., Serga, V., Bandarenka, H., Burko, A., Piskunov, S., Pankratov, V.A., Sarakovskis, A., Popov, A.I., Bocharov, D.V. (2025) Structural and Spectroscopic Characterization of TiO2 Nanocrystalline Materials Synthesized by Different Methods. *Nanomaterials*, 15. DOI: 10.3390/nano15070498.

[21] Sassi, S., Bouich, A., Bessais, B., Khezami, L., Soucase, B.M., Hajjaji, A. (2024) Comparative Analysis of Anodized TiO2 Nanotubes and Hydrothermally Synthesized TiO2 Nanotubes: Morphological, Structural, and Photoelectrochemical Properties. *Materials*, 17. DOI: 10.3390/ma17215182.